

Non-perturbative Many-Body Treatment of Molecular Magnets

Brandon Eskridge and Henry Krakauer

Department of Physics, College of William and Mary, Williamsburg, Virginia 23187, USA

Shiwei Zhang

Center for Computational Quantum Physics,

Flatiron Institute, New York, NY 10010, USA and

Department of Physics, College of William and Mary, Williamsburg, Virginia 23187, USA

(*Electronic address: szhang@flatironinstitute.org)

(*Electronic address: bkeskridge@wm.edu)

Abstract

Molecular magnets have received significant attention because of their potential applications in quantum information and quantum computing. A delicate balance of electron correlation, spin-orbit coupling (SOC), ligand field splitting, and other effects produces a persistent magnetic moment within each molecular magnet unit. The discovery and design of molecular magnets with improved functionalities would be greatly aided by accurate computations. However, the competition among the different effects poses a challenge for theoretical treatments. Electron correlation plays a central role, since d -, or f -element ions, which provide the magnetic states in molecular magnets, often require explicit many-body treatments. SOC, which expands the dimensionality of the Hilbert space, can also lead to non-perturbative effects in the presence of strong interaction. Furthermore, molecular magnets are large, with tens of atoms in even the smallest systems. We show how an *ab initio* treatment of molecular magnets can be achieved with auxiliary-field quantum Monte Carlo (AFQMC), in which electron correlation, SOC, and material specificity are included accurately and on an equal footing. The approach is demonstrated by an application to compute the zero-field splitting of a locally-linear Co^{2+} complex.

PACS numbers:

I. INTRODUCTION

Molecular magnets were first experimentally realized 30 years ago with the magnetic characterization of a Mn_{12} cluster which showed magnetic relaxation times on the order of two months at a temperature of 2K [1]. Since then, broad classes of possible applications for molecular magnet systems have been explored in areas such as high-density classical memory, quantum information [2–7], and chemical catalysis [8], among others. For example, the TbPc_2 molecule has been used to implement Grover’s algorithm within a single molecule [5]. Since the original Mn_{12} cluster, many molecular magnets (often referred to as single-molecule magnets in the literature) have been discovered and designed, based on 3d transition-metal [9–16], lanthanide [17–20], and even actinide ions [21–24]. While most molecular magnets display magnetic hysteresis only at temperatures below a few Kelvin, a dysprosium metallocene cation was recently discovered to display magnetic hysteresis at temperatures of up to 80 K [20]. This represents an encouraging milestone for practical applications of molecular magnets in technology, since magnetic behavior occurs above the temperature of liquid nitrogen. There is significant interest in the design of new molecular magnets both for specific technological applications and fundamental science.

The defining characteristic of molecular magnets is the magnetic bistability that occurs due to their electronic structure. The ground state of molecular magnets must be 2-fold degenerate, at least approximately, with non-zero total angular momentum, along with an energetic barrier that blocks spontaneous reversal of the magnetic moment. The energetic barrier is provided by the zero field splitting (ZFS) that arises due to a combination of spin-orbit coupling (SOC) and symmetry breaking from the ligand field. In the literature, ZFS is often used to refer to the parameters of the phenomenological pseudospin Hamiltonian used to model the effect; in the present work, however, we take ZFS to refer to the energy gaps in the low energy many-body spectrum of the *ab initio* Hamiltonian. Several relevant magnetic relaxation pathways exist for molecular magnets with phonon-mediated processes (Orbach, Raman, and direct electron-phonon scattering) and quantum tunneling of the magnetization most often being the limiting factor in operating temperature. Of course, a complete theoretical investigation of molecular magnets must consider these effects. Much progress has been made in regards to designing efficient molecular magnets in terms of overall strategy for producing efficient molecular magnets based on the choice of magnetic ion, usually a 3d-transition metal or lanthanide, and ligand [25–28]. Accurate and reliable *ab initio* treatments of molecular magnets would greatly facilitate designing molecular magnets and tuning

their properties for specific use.

Molecular magnets pose challenges to explicit many-body treatments due to the very large dimension of the Hilbert space necessary to describe them. While exact solutions to the quantum many-electron problem are possible for small systems, the cost of exact methods scale exponentially in system size, which renders direct applications to typical molecular magnets not possible. Approximate solutions based on density functional theory (DFT) are a natural choice; however, DFT may be inadequate due to the correlated d -, or f -element ions at the core of molecular magnets. In general, Explicit many-body methods will most likely be needed for molecular magnets. The quantum chemistry “gold standard” method, coupled cluster singles doubles with perturbative triples (CCSD(T)), scales as N^7 versus system size, N , making applications to typical molecular magnets challenging. Additionally, while CCSD(T) reliably achieves chemical accuracy for main group chemistry, this is not always the case for 3d-transition metal chemistry [29, 30].

The typical challenges of performing many-body calculations are exacerbated by the inclusion of SOC which is fundamental to the computation of the ZFS. The presence of spin-flip terms in the Hamiltonian expands the dimension of the Hilbert space that must be considered, greatly increasing the high computational cost of explicit many-body methods. In much of the molecular magnet literature, the ZFS gaps and/or pseudospin Hamiltonian parameters are computed in two stages. First, static correlation is accounted for using a non-relativistic or scalar relativistic state-averaged CASSCF (SA-CASSCF) [31, 32] calculation performed in an active space consisting of the magnetically active d -, or f -manifold. Occasionally, a slightly larger active space is used which includes a few orbitals and electrons from the ligand as well. In the SA-CASSCF calculations, care is taken to average over the proper “no SOC” states since the specific states which are chosen for state averaging may influence the results. Dynamic correlation is sometimes approximately accounted for using many-body perturbation theory, usually with 2nd-order N -electron valance perturbation theory (NEVPT2) [33, 34] or 2nd-order complete active space perturbation theory (CASPT2) [35–37]. SOC is then treated in a second stage via either quasi-degenerate perturbation theory (QDPT) [38], or the restricted active space state interaction (RASSI) method [39]. Such two stage approaches to the calculation of the ZFS have been remarkably successful for many 3d-transition metal, and lanthanide complexes.

In this work, we develop a general approach to treat molecular magnets using auxiliary-field quantum Monte Carlo (AFQMC) [40, 41]. We recently incorporated explicit SOC in *ab initio* AFQMC calculations which provides a computational framework where material specificity, both

static and dynamic correlations, and SOC are treated accurately and on an equal footing [42]. AFQMC has demonstrated a high degree of accuracy in correlated electron systems in general, and systems containing 3d-transition metals specifically, as determined by several recent benchmarks [43–46], which, as discussed above, is an important factor for molecular magnets. The calculation of the ZFS in molecular magnets can be performed as a one-shot many-body calculation with no need to perform state-averaging, or to diagonalize the SOC operator in an explicit basis of many-body states. AFQMC has a low order polynomial scaling versus system size (similar to DFT but with a large prefactor), making applications to large systems feasible, even with the inclusion of SOC. Still, the very large Hilbert space dimension of typical molecular magnets makes such applications very computationally demanding. As an additional ingredient, we introduce local embedding [47], which produces an effective Hamiltonian in a basis of local orthonormal orbitals chosen based on local criteria, to focus computational effort on magnetic ions while including much of the ligand as well. The resulting Hamiltonian operates on a significantly reduced Hilbert space, which greatly increases the effective system size that can be treated. The accuracy of local embedding AFQMC can be systematically improved towards full AFQMC treatment of the entire system by increasing the size of the local basis used.

The remainder of the paper is organized as follows. In Section II, we provide a brief summary of the general AFQMC framework, before describing our approach for the non-perturbative treatment of molecular magnet systems using AFQMC. In Section III, we demonstrate the approach by applying it to compute the low-energy many-body spectrum, and ZFS, of the $\text{Co}(\text{C}(\text{SiMe}_2\text{ONaph})_3)_2$ molecule. Comparisons are made with experimental results and other *ab initio* many-body results from the literature [48]. We conclude with some general remarks in Section IV. In the supplemental material, we provide a Python script which reproduces the Hamiltonian used in Section III.

II. THEORY

In this Section, we describe the treatment of molecular magnets using AFQMC including explicit, non-perturbative SOC. We focus specifically on the calculation of the low-energy many-body spectrum, and ZFS gaps. In *ab initio* AFQMC calculations, the many-body Hamiltonian is expressed in the second quantization formalism using a finite basis of orthonormal orbitals as may be obtained from self-consistent field (SCF) calculations. A key component of performing efficient AFQMC calculations in molecular magnets is the production of an effective Hamiltonian

which simplifies the rather complicated Hilbert space of the full system. In Subsection II B, we describe a workflow for the non-perturbative treatment of molecular magnets, at the AFQMC level of theory, including a procedure to produce an interacting second quantized Hamiltonian.

A. Auxiliary-Field Quantum Monte Carlo (AFQMC)

Here, we provide an overview of AFQMC [40, 41]. A recent review outlines the general formalism in detail [49], with a number of technical issues further discussed in Ref. [50]. AFQMC is an orbitally-based many-body method and is formulated in terms of a generic, interacting 2nd quantized Hamiltonian,

$$\hat{H} = \hat{K} + \hat{V} = \sum_{\mu\nu} K_{\mu\nu} \hat{c}_\mu^\dagger \hat{c}_\nu + \sum_{\mu\nu\gamma\delta} V_{\mu\nu\gamma\delta} \hat{c}_\mu^\dagger \hat{c}_\nu^\dagger \hat{c}_\delta \hat{c}_\gamma, \quad (1)$$

where \hat{K} includes all one-body Hamiltonian terms, \hat{V} includes all two-body interaction terms, \hat{c}_μ^\dagger and \hat{c}_μ are the fermionic creation and annihilation operators, respectively, which create/annihilate electrons in a chosen orthonormal basis of single-electron orbitals, and $K_{\mu\nu}$, $V_{\mu\nu\gamma\delta}$ are the matrix of elements of \hat{K} , \hat{V} represented in the orbital basis. Any standard form of the many-electron Hamiltonian can be represented by Eq. 1 including all-electron or pseudopotential Hamiltonians, and relativistic or non-relativistic treatments.

Observables are directly computed using a stochastic representation of many-body states in order to achieve high accuracy at a cost that scales as a low order polynomial. The stochastic representation of a many-body wavefunction, $|\Psi\rangle$, is obtained via projection starting from an initial wavefunction, $|\Psi_I\rangle$, which has nonzero overlap with the target wavefunction. The projection is performed in imaginary time as

$$\lim_{\beta \rightarrow \infty} e^{-\beta \hat{H}} |\Psi_I\rangle = e^{-\tau \hat{H}} e^{-\tau \hat{H}} \dots e^{-\tau \hat{H}} |\Psi_I\rangle \rightarrow |\Psi\rangle, \quad (2)$$

where the total projection time, β , has been divided into small imaginary time steps, τ .

By Thouless' Theorem [51], the operation of the exponential of a one-body operator on a Slater determinant simply produces another Slater determinant; however, the presence of two-body Hamiltonian terms makes the projection nontrivial. To handle general interactions, the projector, $e^{-\tau \hat{H}}$, is cast as a high-dimensional integral as follows. First, the electron-electron interaction term is factored into a quadratic form of one-body operators,

$$\hat{V} = \sum_{\gamma} \hat{v}_{\gamma}^2, \quad (3)$$

where \hat{v}_γ are one-body operators which are usually obtained from a modified Cholesky decomposition [52]. The set of \hat{v}_γ are truncated based on a small cutoff threshold, $\delta_{Chol.}$, which introduces a systematically improvable approximation. Second, a Trotter-Suzuki [53, 54] decomposition is performed,

$$e^{-\tau\hat{H}} \approx e^{-\tau\hat{K}/2} e^{-\tau\sum_\gamma \hat{v}_\gamma^2} e^{-\tau\hat{K}/2} + \mathcal{O}(\tau^3), \quad (4)$$

followed by a Hubbard–Stratonovich transformation [55, 56] of $e^{-\tau\sum_\gamma \hat{v}_\gamma^2}$. The projector is then given by,

$$e^{-\tau\hat{H}} \approx \int d\boldsymbol{\sigma} P(\boldsymbol{\sigma}) B(\boldsymbol{\sigma}) + \mathcal{O}(\tau^3), \quad (5)$$

where $\boldsymbol{\sigma}$ is a vector containing auxiliary-fields, $P(\boldsymbol{\sigma})$ is a normal distribution function, and $B(\boldsymbol{\sigma})$ is given by

$$B(\boldsymbol{\sigma}) = e^{-\tau\hat{K}/2} e^{\sqrt{\tau}\boldsymbol{\sigma}\cdot\hat{\mathbf{v}}} e^{-\tau\hat{K}/2}, \quad (6)$$

where $\hat{\mathbf{v}}$ is the vector of one-body operators defined implicitly by Eq. 3. Since $B(\boldsymbol{\sigma})$ is simply a product of exponentials of one-body operators, it can be easily applied to Slater determinants and the integral is evaluated by sampling auxiliary-fields from $P(\boldsymbol{\sigma})$ at each imaginary time step. Many-body states are represented in an over-complete basis of non-orthogonal Slater determinant random walkers as

$$|\Psi\rangle \doteq \sum_k |\Phi_k\rangle, \quad (7)$$

where $|\Phi_k\rangle$ is a single Slater determinant random walker, and k runs over all walkers. Thus, the projection has been cast as a random walk in nonorthogonal Slater determinant space.

The sign/phase problem, which is a generic problem that effects all fermionic quantum Monte Carlo approaches, is controlled by the phaseless approximation in *ab initio* AFQMC calculations [40]. The phase problem arises from the fact that physical observables are invariant under an arbitrary complex phase of the wavefunction from which they are computed. As the random walk progresses, walkers accumulate a random phase relative to each other due to the, generally, complex-valued projector. An importance sampling transformation based on the overlap of individual walkers with a trial wavefunction, $|\Psi_T\rangle$, is used to cast the random walks in a fixed gauge choice, which provides the theoretical basis to control this problem [57]. The trial wavefunction

is an approximation to the target many-body state, and must have non-zero overlap with the desired exact many-body state. With importance sampling, the Monte Carlo representation of the many-body wavefunction becomes,

$$|\Psi\rangle \doteq \sum_k w_k |\Phi_k\rangle, \quad (8)$$

where w_k is a weight which is accumulated over the course of the random walk based on a chosen importance function, I , at projection step n as $w_k^{(n)} = I(\boldsymbol{\sigma}, \Phi_k^{(n-1)}) w_k^{(n-1)}$. Random walkers are still free to diffuse across the entire complex plane defined by $\langle \Psi_T | \Phi_k \rangle$, allowing a finite density of walkers to accumulate at the origin, causing walker weights to diverge as the walk progresses. The phase problem is then eliminated by projecting each individual walker onto an evolving line in the complex plane. This is achieved by multiplying each walker by $\max\{0, \cos(\Delta\theta)\}$, where $\Delta\theta$ is the phase of $\langle \Psi_T | \Phi_k \rangle / \langle \Psi_T | \Phi_{k-1} \rangle$. The phaseless approach introduces a bias which can be controlled by the quality of the trial wavefunction.

The most straight-forward application of AFQMC is the computation of the ground state energy. Excited state AFQMC calculations are possible if a suitable trial wavefunction is used [58]. This typically requires a multideterminant trial wavefunction as may be obtained from CASSCF or other approaches. Other more advanced projection methods are possible [59] but we will limit ourselves to the more conventional approach with multi-determinants.

SOC can be treated explicitly in *ab initio* AFQMC calculations [42] since the SOC term, $\hat{K}^{soc} \equiv \hat{\mathbf{W}}^{soc} \cdot \hat{\mathbf{S}}$, is of a general one-body form as in generalized Hartree-Fock. Several choices of $\hat{\mathbf{W}}^{soc}$ are possible ranging from all-electron relativistic Hamiltonians to formally non-relativistic model Hamiltonians based on relativistic pseudopotentials (PSPs) or effective core potentials (ECPs). Explicitly, the 2nd-quantized Hamiltonian with SOC in a spin-orbital basis is given by

$$\hat{H}^{soc} = \sum_{\mu\nu} \left(K_{\mu\nu} + K_{\mu\nu}^{soc} \right) \hat{c}_\mu^\dagger \hat{c}_\nu + \sum_{\mu\nu\gamma\delta} V_{\mu\nu\gamma\delta} \hat{c}_\mu^\dagger \hat{c}_\nu^\dagger \hat{c}_\delta \hat{c}_\gamma, \quad (9)$$

where $K_{\mu\nu}^{soc} = [W^z S_z + W^+ S_+ + W^- S_-]_{\mu\nu}$. The greek indices, μ, ν, γ, δ correspond to spin-orbitals of the form $\chi_{\mu=(i,\sigma)} = \phi_i(\vec{r}) |\sigma\rangle$, where $\phi_i(\vec{r})$ are spatial orbitals, and $|\sigma\rangle$ are eigenstates of the single-particle \hat{s}_z operator.

The AFQMC procedure is formally unchanged by the inclusion of explicit SOC; however, a few practical adaptations must be made. With no SOC, the HS propagator, $B(\boldsymbol{\sigma})$, of Eq 6 can be factorized

$$B(\boldsymbol{\sigma}) = B^\uparrow(\boldsymbol{\sigma}) \otimes B^\downarrow(\boldsymbol{\sigma}), \quad (10)$$

where $B^\uparrow(\sigma)$ ($B^\downarrow(\sigma)$) operates only on the up (down) spin sector, and Slater determinant random walkers are given as

$$|\Phi_i\rangle = |\Phi_i^\uparrow\rangle \otimes |\Phi_i^\downarrow\rangle. \quad (11)$$

With SOC, the HS projector explicitly mixes spins and has the form

$$B^G(\sigma) = \begin{bmatrix} B^\uparrow(\sigma) & B^+(\sigma) \\ B^-(\sigma) & B^\downarrow(\sigma) \end{bmatrix}, \quad (12)$$

where the spin-flip propagators $B^{+/-}(\sigma) = \text{Exp}[-\tau\hat{W}^{+/-}]$ are Hermitian conjugates of each other, and $B^\uparrow(\sigma)$ ($B^\downarrow(\sigma)$) includes both the usual spin-independent terms, and the z-projection of the SOC term. Generalized Slater determinant random walkers

$$\Phi^G = \begin{bmatrix} \Phi^{\uparrow\uparrow} & \Phi^{\uparrow\downarrow} \\ \Phi^{\downarrow\uparrow} & \Phi^{\downarrow\downarrow} \end{bmatrix}, \quad (13)$$

are used during the AFQMC projection. Thus, SOC is included exactly and on an equal footing with electron correlation. The effective system size is doubled compared with treatments that neglect SOC.

B. Treatment of molecular magnets

In this subsection, we describe the treatment of molecular magnets at the many-body level of theory, including explicit SOC, electron correlation, and ligand field effects. The basic idea is to produce a 2nd quantized Hamiltonian from which the low energy spectrum may be computed using AFQMC either with or without SOC. Figure 1 includes a schematic representation of the high-level workflow. In the remainder of this section, we describe each step in the workflow using the schematic as a guide.

Our procedure begins with an initial Hartree-Fock or DFT calculation, as indicated in the light green box of Fig. 1. This is performed in order to generate an orbital basis, and an electron density, for subsequent local embedding (DFT+ U type calculations can also be used). This can be accomplished with calculations that neglect SOC since typical ligands for molecular magnets consist of light atoms, or atoms which are closed-shell. For ligands containing heavy elements, such as Br, I, or Bi [60, 61], it will be useful to include SOC from the outset. Here, we used spin restricted open-shell Kohn-Sham (ROKS) DFT which provides a convenient starting point

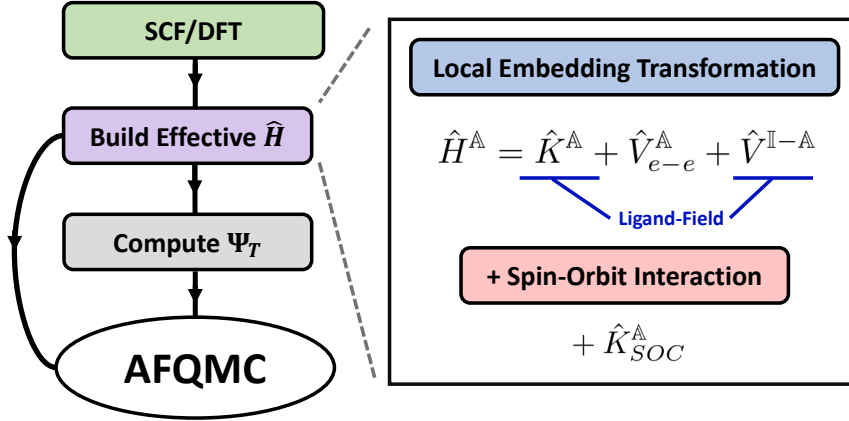


FIG. 1: Schematic of the molecular magnet treatment workflow. The workflow proceeds from top to bottom. Boxes represent specific steps in the procedure and solid black lines with arrows indicate that the output from one step is used as an input to another. Dotted gray lines indicate a “breakout” of the purple box into two essentially independent substeps. Each step of the workflow is outlined in the main text.

for local embedding. However, spin unrestricted Kohn-Sham (UKS) or generalized Kohn-Sham (GKS) DFT could be used instead, if desired.

The next step, corresponding to the purple box in Figure 1, is to construct an effective Hamiltonian for the molecular magnet system. We require a Hamiltonian which captures material-specific ligand field effects, SOC, and electron correlation. This is achieved in two steps, as indicated by the dotted breakout section of Fig. 1. First, local embedding is employed, as described below, to build an effective Hamiltonian describing the magnetically active ion(s) in the molecular magnet and which accounts for ligand field effects. Second, a SOC operator, which operates on the same Hilbert space as the effective Hamiltonian, is constructed and added to the effective Hamiltonian. We describe both of these steps below. Of course, one can perform calculations with no SOC by simply neglecting the second step.

We outline the local embedding approach we use in AFQMC [47, 62]. The crux of local embedding is a separability approximation of the many-body wavefunction, $|\Psi\rangle$, into an active and an inactive part,

$$|\Psi\rangle \approx \mathcal{A}(|\Psi^{\text{I}}\rangle \otimes |\Psi^{\text{A}}\rangle), \quad (14)$$

where $|\Psi^{\text{I}}\rangle$ is a wavefunction in the inactive space, $|\Psi^{\text{A}}\rangle$ is the active space many-body wavefunc-

tion, and \mathcal{A} is an antisymmetrizer. The choice of \mathbb{A} and \mathbb{I} can lead to different forms of embedding, and here they are chosen based on local criteria. This approximation allows the energy of the full Hamiltonian to be mapped onto an effective embedding Hamiltonian:

$$\langle \Psi | \hat{H} | \Psi \rangle = \langle \Psi^{\mathbb{A}} | \hat{H}^{\mathbb{A}} | \Psi^{\mathbb{A}} \rangle, \quad (15)$$

where $\hat{H}^{\mathbb{A}}$ is the embedding Hamiltonian which operates only in \mathbb{A} similar to the standard frozen core approximation. This condition leads to the following explicit form of the embedding Hamiltonian,

$$\hat{H}^{\mathbb{A}} = \sum_{ij \in \mathbb{A}} K_{ij} \hat{c}_i^\dagger \hat{c}_j + \sum_{ijkl \in \mathbb{A}} V_{ijkl} \hat{c}_i^\dagger \hat{c}_j^\dagger \hat{c}_l \hat{c}_k + \sum_{ij \in \mathbb{A}} V_{ij}^{\mathbb{I}-\mathbb{A}} \hat{c}_i^\dagger \hat{c}_j + E_{\mathbb{I}}, \quad (16)$$

where the first two terms are the one-, and two-body terms in the full Hamiltonian restricted to orbitals within \mathbb{A} , $E_{\mathbb{I}}$ is a constant contribution from the energy of the inactive part, and $\hat{V}^{\mathbb{I}-\mathbb{A}} = \sum_{ij \in \mathbb{A}} V_{ij}^{\mathbb{I}-\mathbb{A}} \hat{c}_i^\dagger \hat{c}_j$ is a one-body operator which captures the interaction between active and inactive electrons. Formally, $\hat{V}^{\mathbb{I}-\mathbb{A}}$ is an energy consistent, non-local pseudopotential which is computed for the specific system at hand, avoiding transferability errors. The combination of \hat{K} , restricted to \mathbb{A} , and $\hat{V}^{\mathbb{I}-\mathbb{A}}$ describe the symmetry of the full ligand. Therefore, a small active space focused tightly on a magnetic ion is directly influenced by the ligand field at the many-body level of theory.

The partition between \mathbb{A} and \mathbb{I} is defined in terms of a chosen set of active/inactive local orbitals. Orbitals are assigned to the active space if their centroid is localized within a chosen localization radius of the strongly-correlated center(s), and a separate localization radius is used for occupied orbitals, R_o , and for virtual orbitals, R_v . The accuracy of the approximation can be dialed up by increasing R_o and R_v and it was previously shown that, for fixed R_o , the absolute AFQMC energy converges in R_v at $R_v = R_o + C$ with C being a system-dependent constant typically ranging from 2-6 Bohr [47]. However, relative energies, such as the zero-field splitting (ZFS), converge more rapidly, allowing for smaller choices of C . In initial test cases, local embedding was observed to reduce the computational cost of some calculations by orders of magnitude compared with AFQMC performed on the full Hilbert space.

For the computation of the ZFS gaps, AFQMC calculations are performed with an explicit SOC operator included in the Hamiltonian. An explicit spin-orbital basis, $\{|\chi_\mu\rangle\}$, is constructed from the set of active local orbitals corresponding to \mathbb{A} . The second quantized SOC operator can be constructed directly in the spin-orbital basis as

$$\hat{K}_{\mu\nu}^{soc} = \langle \chi_\mu | \hat{W}^{soc} \cdot \hat{S} | \chi_\nu \rangle, \quad (17)$$

which is added to \hat{H}^{A} (also transformed to the spin-orbital basis). Several choices of *ab initio* SOC operators are available in the literature, including all-electron and PSP formalisms. In the case of all-electron relativistic Hamiltonians, the Breit interaction, which is a spin-dependent two-body interaction, is often modeled by an approximate one-body operator. This is often done via the spin-orbit mean-field (SOMF) approximation [63], in which the full Breit interaction is replaced with a Fock-like operator constructed from a given electron density, although other approximations exist as well [64]. A detailed discussion of the accuracy of such effective one-body approximations to the Breit interaction is beyond the scope of the present work, but there are indications from perturbative treatments of molecular magnets [65] that such approximations provide a reasonable description. In the case of PSP formalisms, contributions from the Breit interaction are implicitly accounted for, again as an effective one-body contribution, if the PSP is fit using reference data which accounts for the Breit interaction, as is quite common for fully relativistic PSPs. Equation 17 is consistent with any effective one-body treatment of SOC, but we adopt the use of relativistic PSPs which have demonstrated a high degree of accuracy compared with experiment and which also have the advantage of allowing SOC to be included selectively for atoms where SOC effects are expected to be most important - i.e. for heavy and/or magnetically active ions.

The next step in the workflow, indicated by the light gray box in Figure 1, is to compute trial wavefunctions for AFQMC. The embedding Hamiltonian (Eq. 16) is used for this purpose. (In Sec. III we perform calculations both with and without SOC. The trial wave function is generated with or without SOC, consistently with the target AFQMC calculation.) For general excited state calculations, such as the ZFS, targeting the correct quantum numbers and symmetry is as important as the accuracy (as judged by the variational energy, for example). Many approaches can be used to compute the trial wave function [50]. In the present work, we used truncated multi-determinant expansions computed using semistochastic heatbath CI (SHCI) [66–68], including explicit SOC where needed. We used a small active space for SHCI which focuses on the magnetically active electrons. We note that SHCI can treat much larger active spaces than those used here, but that is not needed for the present purpose since the AFQMC results converge quickly with respect to the truncated trial wave function.

In molecular magnets, the z-projection of the total angular momentum, \hat{J}_z , is often an approximately good quantum number. While it is possible to construct rigorous many-body eigenstates of the \hat{J}_z operator for a particular system, these may not correspond to approximate eigenstates of the Hamiltonian in general and, therefore, may perform poorly as trial wavefunctions for AFQMC. Al-

ternatively, one may utilize a complete set of \hat{J}_z eigenstates, $\{|\Phi_i^{M_J}\rangle\}$, where M_J is the eigenvalue corresponding to \hat{J}_z and i is an index within the M_J manifold, as a basis in which to characterize the approximate \hat{J}_z quantum number label via projection. An arbitrary many-body wavefunction, $|\Psi\rangle$, may be expressed as

$$|\Psi\rangle = \sum_{M_J=-J}^J \sum_{i \in M_J} C_i^{M_J} |\Phi_i^{M_J}\rangle, \quad (18)$$

where $C_i^{M_J} = \langle \Phi_i^{M_J} | \Psi \rangle$. The total weight of $|\Psi\rangle$ which resides within a particular M_J -manifold is given by

$$W^{M_J} = \sum_{i \in M_J} |C_i^{M_J}|^2. \quad (19)$$

Approximate M_J labels are then assigned based on the weights as determined by Eq. 19, but only if such an assignment can be made unambiguously.

Our procedure to assign quantum numbers to each trial wavefunction, when possible, is as follows. While the dimension of a complete set of \hat{J}_z eigenstates is exponentially large, the angular momentum is determined by only a handful of d -, or f -electrons in practice. Diagonalizing \hat{J}_z only within the corresponding manifold(s) provides meaningful M_J labels while limiting the dimension of the basis of M_J states to a routinely manageable size. In this case, the equality in Eq. 18 no longer holds and the accuracy of the approximation can be measured by comparing the total weight of the original wavefunction to that of the M_J -decomposed wavefunction. In the present work, all SHCI wavefunctions retained an average total weight of 0.9998(1) after being projected into the M_J basis. In the absence of SOC, a similar procedure can be used to assign M_L labels by diagonalizing \hat{L}_z instead of \hat{J}_z . We emphasize that the trial wavefunctions used in AFQMC calculations are truncated SHCI wavefunctions, which retain only $\mathcal{O}(50)$ determinants; no attempt was made to force particular quantum numbers in the truncated trial wave function.

In the final step, AFQMC calculations of the ground state and low-lying excited states are performed using the local embedding Hamiltonian either with (without) SOC, and selecting trial wavefunctions based on their approximate M_J (M_L) value. The approach can be applied to any molecular magnet system including those with several magnetic centers (with only minor modifications). Thus, the AFQMC method provides a general framework for the non-perturbative simulation of molecular magnets. We demonstrate this framework in Sec. III below.

III. APPLICATION TO A LINEAR CO²⁺ COMPLEX

The Co(C(SiMe₂ONaph)₃)₂ molecule was recently synthesized and experimentally characterized, displaying magnetic hysteresis at temperatures of up to 5K [48]. It is, to our knowledge, the current record holder for ZFS gap among single ion molecular magnets based on 3d transition metals. The large ZFS gap is due to unquenched orbital angular momentum in the ground state, which is unusual for 3d-element complexes. The Co²⁺ ion at the core of the Co(C(SiMe₂ONaph)₃)₂ molecule has similar electronic structure to a Co²⁺ ion adsorbed on the surface of MgO [69], which also displays unquenched orbital angular momentum in the ground state.

The weak S_6 ligand field and the locally-linear coordination environment of the Co²⁺ ion at the center of the Co(C(SiMe₂ONaph)₃)₂ molecule lead to a $C_{\infty v}$ pseduosymmetry which provides approximate symmetry labels each corresponding to a well defined eigenvalue of \hat{L}_z . Neglecting SOC, a Co²⁺ ion in vacuum has a ⁴F ground state. Under a $C_{\infty v}$ ligand field, the ⁴F state is split into ⁴Σ, ⁴Π, ⁴Δ, and ⁴Φ where each level is two-fold degenerate in orbital degrees of freedom except for ⁴Σ, which is non-degenerate. Even a modestly strong $C_{\infty v}$ field would typically lead to a ⁴Σ ground state; however, the weak ligand field in Co(C(SiMe₂ONaph)₃)₂ leads to a ⁴Φ ground state instead. If SOC is included, \hat{L}_z no longer provides a good quantum number and the ⁴Φ state is split into eigenstates of \hat{J}_z , which range from $M_J = 9/2$ to $M_J = 3/2$. The ground state of Co(C(SiMe₂ONaph)₃)₂ has $M_J = 9/2$ as determined by DC magnetic susceptibility data from the literature, and the first excitation ZFS gap of 450 cm^{-1} is attributed to an excitation to the $M_J = 7/2$ level. Since Co²⁺ is a Kramer's ion, Co(C(SiMe₂ONaph)₃)₂ has exact two-fold degeneracy regardless of the ligand field symmetry. In our discussions below, $C_{\infty v}$ and M_J labels are only approximate and are determined as described in Sec. II B.

We apply the general computational framework described in Sec. II B to compute the low-energy spectrum of Co(C(SiMe₂ONaph)₃)₂, both with and without SOC. ZFS gaps are taken directly from the low energy spectrum computed with SOC. The Co ion is treated with the CRENBL PSP (which is based on fully relativistic reference data), using the corresponding uncontracted Gaussian primitive basis [70]. All other atoms are treated with the non-relativistic all-electron Hamiltonian using the standard cc-pVDZ basis for C, O, and Si and the STO-6G basis for H. We verified that the cc-pVDZ basis for ligand atoms is adequate for the calculations performed here.

The experimentally observed geometry of the Co(C(SiMe₂ONaph)₃)₂ molecule [48] is shown in panel a) of Fig. 2. The ligand has S_6 symmetry; however, all calculations were performed

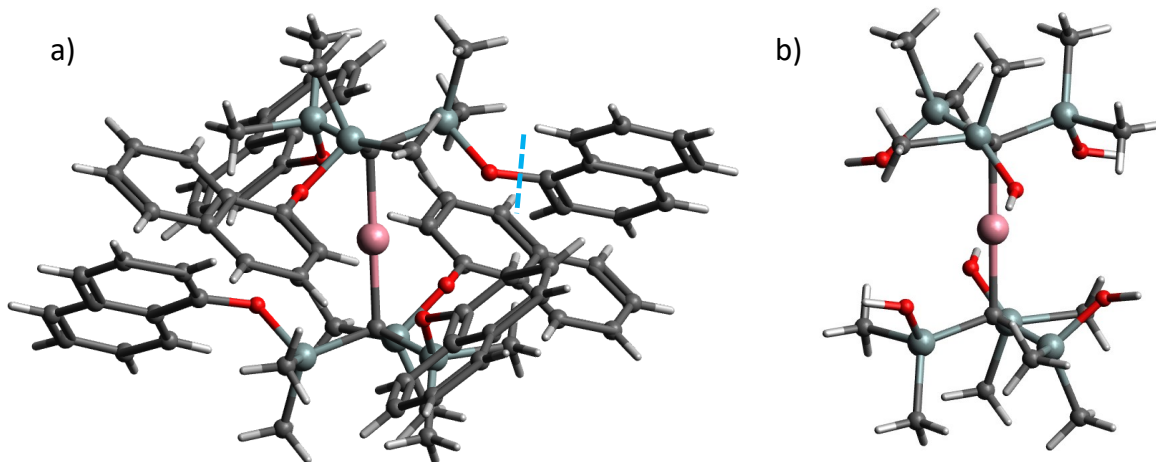


FIG. 2: Molecular geometry of the $\text{Co}(\text{C}(\text{SiMe}_2\text{ONaph})_3)_2$ molecule. Atomic species are identified by color. Co atoms are pink, Si are pale green, O are red, C are dark gray, and H are light gray/white. Panel a) shows the full molecule as determined by x-ray diffraction experiments from the literature [48]. The molecule has S_6 symmetry, and the central C-Co-C axis is approximately linear. Panel b) shows the simplified model used in the present work. The six naphthol (C_{10}H_7) units in panel a) are replaced with an H-termination, holding the Si-O-H angle unchanged. One of the cut O-C bonds is indicated by a light blue dotted line in panel a).

without imposing point-group symmetry. To assist in converging the initial DFT calculations, we replaced each of the six naphthol (“Naph” = C_{10}H_7) units with a hydrogen termination using an O-H bondlength of 1.04 \AA and maintaining the original Si-O-C bond angle; the simplified geometry, $\text{Co}(\text{C}(\text{SiMe}_2\text{OH})_3)_2$, is illustrated in panel b) of Fig. 2. No further geometry optimization was performed on $\text{Co}(\text{C}(\text{SiMe}_2\text{OH})_3)_2$. Results in the literature showed that the ZFS computed for $\text{Co}(\text{C}(\text{SiMe}_2\text{ONaph})_3)_2$ and the ZFS computed for a model in which naphthol units were replaced by a methyl group were essentially identical level-by-level, with a maximum deviation of 14 cm^{-1} but with most levels agreeing to within 3 cm^{-1} [48]. This suggests that the ZFS is not sensitive to the details of the ligand for this particular complex, which is unsurprising given the very weak ligand field strength.

Initial DFT calculations were performed using the PBE0 functional and including only the scalar relativistic part of the Co PSP with no SOC. A local embedding Hamiltonian was constructed as described in Sec. II B using the PBE0 solution, Foster-Boys localized [71] restricted open-shell Kohn-Sham (ROKS) orbitals as a basis, and localization radii $(R_o, R_v) = (2.8, 5.4)$

atomic units centered at the Co ion. This choice of localization radii yields an active space which includes all Co occupied and virtual orbitals, and some ligand orbitals, for a total of 99 spatial orbitals, or 198 spin-orbitals. The $3s$, $3p$ and $3d$ electrons belonging to the Co^{2+} ion are all included in the active space, as well as a total of 4 additional electrons from neighboring C atoms, for a total of 19 active electrons. We checked that the choice of (R_o, R_v) is sufficient for the purpose of computing the ZFS levels in $\text{Co}(\text{C}(\text{SiMe}_2\text{OH})_3)_2$.

We computed trial wavefunctions for AFQMC using SHCI as implemented in the code ‘‘Dice’’ [66–68]. We performed ROHF on the embedding Hamiltonian with no SOC to provide a reference determinant for SHCI, and to define the Co $3d$ -orbitals. SHCI calculations, both with and without SOC, were performed for a small active space consisting of 7 orbitals and 11 electrons, which include both the $3d$ orbitals/electrons and some ligand orbitals/electrons; in the SHCI, a variational cutoff of $1.0\text{E-}5$ was used. We then truncate the SHCI wavefunction by discarding determinants with small weights using a truncation threshold of 0.001, to obtain the trial wavefunctions for AFQMC. We assigned labels to each trial wavefunction corresponding to \hat{J}_z and \hat{L}_z for calculations performed with SOC and without SOC, respectively, as described in Sec. II B. We confirmed that AFQMC maintains the same M_J (M_L) labels as the trial wavefunctions.

The low energy many-body spectrum of $\text{Co}(\text{C}(\text{SiMe}_2\text{OH})_3)_2$ computed from AFQMC is shown in panel a) of Fig. 3. Results are organized into two columns. The left column, labelled ‘‘No SOC’’, is for a Hamiltonian with only the scalar relativistic PSP of Co, without SOC. The AFQMC ground state from the ‘‘No SOC’’ column is used as an absolute energy reference for all of panel a). Symmetry labels in the ‘‘No SOC’’ column correspond to approximate $C_{\infty v}$ labels. The right column, labelled ‘‘SOC’’, is for a Hamiltonian which contains both the scalar relativistic and the SOC parts of the Co PSP. In all panels of Fig. 3, red horizontal lines are AFQMC energy levels, and boxes indicate the stochastic uncertainties. Besides AFQMC results, we also show the results of the modest SHCI calculation from which the trial wavefunction was generated, as well as a SA-CASSCF(50,7e) + QDPT result from the literature [48], for reference. The experimentally measured ZFS [48] of 450 cm^{-1} , determined to be from the gap between an $M_J = 9/2$ ground state and $M_J = 7/2$ first excited state, is also included in panel b).

The ‘‘No SOC’’ spectrum in Fig. 3 corresponds to all levels that nominally originate from the ^4F ground state of a Co^{2+} ion in vacuum split by a $C_{\infty v}$ ligand field. The ground state is a $^4\Phi$ state, with unquenched orbital angular momentum, which would be doubly degenerate under perfect $C_{\infty v}$ symmetry; however, the system has only S_6 symmetry. A small gap of

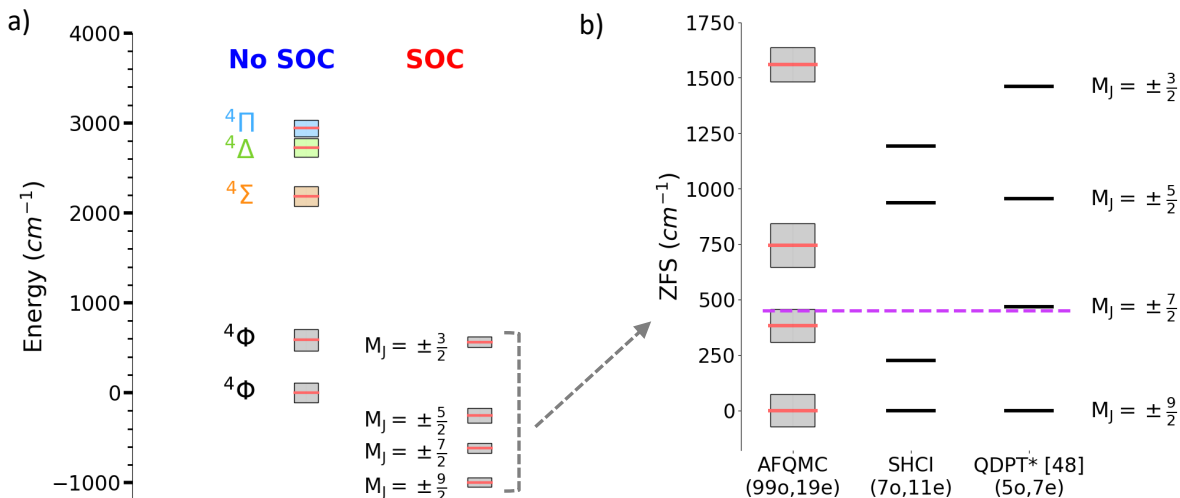


FIG. 3: AFQMC results for the $\text{Co}(\text{C}(\text{SiMe}_2\text{OH})_3)_2$ molecule. Panel a) shows energy levels with (right column) and without (left column) SOC. Red horizontal lines are AFQMC energies and shaded boxes are the stochastic uncertainty. Colored boxes in the entire figure correspond to the approximate $C_{\infty v}$ labels of “No SOC”. Approximate symmetry labels (see main text) are displayed next to the corresponding AFQMC energy level. The AFQMC energies are plotted on the same absolute scale using the “No SOC” $^4\Phi$ ground state energy ($-2881.97934 E_{Ha}$) as a reference. Panel b) contains the ZFS computed with AFQMC, corresponding to the “SOC” column in panel a). For reference, the ZFS computed in the SHCI(7o,11e) calculations, from which we obtain a truncated trial wavefunction for AFQMC, is also shown, together with the result from SA-CASSCF(5o,7e) + QDPT [48] (labelled “QDPT* (5o,7e)”). The experimentally observed ZFS is plotted as a purple horizontal dotted line.

$590(178) \text{ cm}^{-1}$ exists between the ground state and its approximate $^4\Phi$ pair. Nonrelativistic state-averaged CASSCF(5o,7e) calculations order the states as $^4\Phi$, $^4\Sigma$, $^4\Delta$, then $^4\Pi$ [48], similar to our AFQMC results. The $^4\Delta$ and $^4\Pi$ states computed with AFQMC are separated by only $217(138) \text{ cm}^{-1}$. The total spread of the splitting of a hypothetical 4F state under the ligand field in $\text{Co}(\text{C}(\text{SiMe}_2\text{OH})_3)_2$ is $2717(281) \text{ cm}^{-1}$, similar to the estimate of 2768 cm^{-1} obtained from non-relativistic SA-CASSCF(5o,7e)+NEVPT2 [48]. The relatively small spread reflects the weak ligand field strength.

In Fig. 3 the low energy many-body spectrum of $\text{Co}(\text{C}(\text{SiMe}_2\text{OH})_3)_2$, with SOC included, is shown in the right column of panel a). The AFQMC calculations were run longer for “SOC”

than for “No SOC” (beyond the expected increase in computational demand due to the doubling of the Slater determinants), in order to gather more statistics to resolve the small energy scales. All states which originate from both of the $^4\Phi$ states in the “No SOC” column are included. All levels computed with SOC are two-fold degenerate due to time reversal symmetry, and AFQMC was run for only one of the two states. AFQMC predicts an $M_J = 9/2$ ground state, consistent with experiment. The effect from SOC is seen to contribute on roughly the same energy scale as the splittings induced by the ligand field.

Panel b) in Fig. 3 shows a zoomed in view of the computed ZFS, with respect to the energy of the ground state, $M_J = 9/2$. The ZFS computed using SHCI(7o,11e) correspond to the calculations used to obtain trial wavefunctions for AFQMC and are derived from the variational energy of the SHCI wavefunctions. For comparison, we included the ZFS computed using SA-CASSCF(5o,7e) + QDPT, as well as experimental values, all taken from Ref. [48]. The experimental result, displayed as a purple horizontal dotted line, is from variable-field far-infrared spectroscopy, covering an energy range of 30-600 cm^{-1} , and represents a direct measure of the ZFS. We note that the energy range explored by experiment does not reach the next gap predicted by either AFQMC or by SA-CASSCF(5o,7e)+QDPT. The gap between the $M_J = 9/2$ ground state and the $M_J = 7/2$ state computed by AFQMC is 382(74) cm^{-1} , where the error bar is the joint statistical uncertainty of the two separate calculations. This agrees with the experimentally observed value of 450 cm^{-1} . SA-CASSCF(5o,7e) + QDPT yields an excitation gap of 468 cm^{-1} , which agrees remarkably well with experiment. The spectrum computed from AFQMC provides a useful benchmark. It is interesting to note that, in addition to the first excitation, SA-CASSCF(5o,7e) + QDPT also yields a spectrum in good agreement with AFQMC, over-estimating the second excitation slightly.

IV. CONCLUSION AND OUTLOOK

We have developed a general non-perturbative approach to treat molecular magnets using AFQMC, in which material specificity, static and dynamic electron correlation, and SOC are treated accurately and on an equal footing. As a first application, we test the method on a slightly simplified model of the $Co(C(SiMe_2ONaph)_3)_2$ molecule. *Ab initio* AFQMC incorporating SOC and treating the interaction in a large active space yields a ZFS gap of 382(74) cm^{-1} , between the $M_J = 9/2$ ground state and the $M_J = 7/2$ excited state, consistent with the experimental value of 450 cm^{-1} . The computed low-lying excitations can serve as a useful benchmark for future work

in this system and for method developments.

We expect this approach to be applicable to many other related systems for high accuracy, predictive calculations. A number of methodological improvements can be made to further improve the computational efficiency, in order to treat even larger systems or target higher statistical accuracies. The $\text{Co}(\text{C}(\text{SiMe}_2\text{ONaph})_3)_2$ molecule has one of the largest known ZFS gaps of 3d-transition metal based molecular magnets. Most others have ZFS gaps which are smaller by at least a factor of 2-3, often more. Here, we computed the ZFS by performing independent AFQMC calculations for each M_J level; Sufficient resolution was achieved with this approach. For computing the ZFS for general molecular magnets, a higher resolution can be reached via correlated sampling, which directly computes relative energies, such as the ZFS gaps, with significantly reduced Monte Carlo noise [72].

We computed the low-energy many-body spectrum of the $\text{Co}(\text{C}(\text{SiMe}_2\text{OH})_3)_2$ molecule. AFQMC can also be used to directly compute general observables, such as forces, electron density, and phonon/vibrational modes, via the back-propagation algorithm [73, 74]. The use of back-propagation would follow essentially the same procedure as shown in Fig. 1 where the final step would be AFQMC with back-propagation instead of the energy-only calculations performed here. This is, of course, highly desirable since structural details (e.g. ligand symmetry) and vibrational properties are key elements of molecular magnet design. Much of the molecular magnet literature relies upon the experimentally measured geometry of molecular magnets in order to perform ZFS calculations. AFQMC offers a direct route to the *ab initio* prediction of equilibrium geometries as has been demonstrated in solids [75] which would greatly assist in the design of new molecular magnets.

Molecular magnets are very large both in terms of their spatial extent, and the dimension of the corresponding many-body Hilbert space. In the procedure described in Sec. II B, local embedding AFQMC [47] is employed as a way to reduce the size of the active space while retaining system-specific details. In the case of $\text{Co}(\text{C}(\text{SiMe}_2\text{OH})_3)_2$, local embedding led to a reduction in computational cost by a factor of approximately 5000 relative to a hypothetical AFQMC calculation performed using the full Hilbert space. Local embedding benefits greatly from a cancellation of errors in relative energy calculations, such as for the ZFS, and is systematically improvable towards full AFQMC by increasing the localization radii (R_o, R_v). Direct AFQMC computations of the full molecular magnets without embedding is also rapidly becoming feasible, by taking advantage of GPU-acceleration [76, 77] and efficient multi-determinant trial wavefunction algorithms [50, 78].

The combination of effective embedding approaches with these advances in computational efficiency will spur a large number of applications in molecular magnets and beyond.

Acknowledgments

We thank Kyungwha Park, and James Shee for helpful discussions. We also acknowledge support from the U.S. Department of Energy (DOE) under grant DE-SC0001303. The Flatiron Institute is a division of the Simons Foundation. The authors acknowledge William & Mary Research Computing for providing computational resources and/or technical support that have contributed to the results reported within this paper. URL: <https://www.wm.edu/it/rc>

-
- [1] R. Sessoli, D. Gatteschi, A. Caneschi, and M. A. Novak, *Nature* **365**, 141 (1993).
 - [2] R. Vincent, S. Klyatskaya, M. Ruben, W. Wernsdorfer, and F. Balestro, *Nature* **488**, 357 (2012).
 - [3] M. Urdampilleta, S. Klyatskaya, M. Ruben, and W. Wernsdorfer, *Phys. Rev. B* **87**, 195412 (2013).
 - [4] S. Thiele et al., *Science* **344**, 1135 (2014).
 - [5] C. Godfrin et al., *Phys. Rev. Lett.* **119**, 187702 (2017).
 - [6] A. Gaita-Ariño, F. Luis, and E. Hill, S. and Coronado, *Nature Chemistry* **11**, 301 (2019).
 - [7] S. L. Bayliss et al., *Science* **370**, 1309 (2020).
 - [8] J. L. S. Milani et al., *Dalton Trans.* **51**, 12258 (2022).
 - [9] D. E. Freedman et al., *Journal of the American Chemical Society* **132**, 1224 (2010), PMID: 20055389.
 - [10] W. H. Harman et al., *Journal of the American Chemical Society* **132**, 18115 (2010), PMID: 21141856.
 - [11] D. Weismann et al., *Chemistry – A European Journal* **17**, 4700 (2011).
 - [12] J. M. Zadrozny and J. R. Long, *Journal of the American Chemical Society* **133**, 20732 (2011), PMID: 22142241.
 - [13] J. M. Zadrozny et al., *Nature Chemistry* **5**, 577 (2013).
 - [14] J. M. Zadrozny et al., *Chem. Sci.* **4**, 125 (2013).
 - [15] M. S. Fataftah, J. M. Zadrozny, D. M. Rogers, and D. E. Freedman, *Inorganic Chemistry* **53**, 10716 (2014), PMID: 25198379.
 - [16] K. E. R. Marriott et al., *Chem. Sci.* **6**, 6823 (2015).

- [17] N. Ishikawa, M. Sugita, T. Ishikawa, S.-y. Koshihara, and Y. Kaizu, *Journal of the American Chemical Society* **125**, 8694 (2003), PMID: 12862442.
- [18] J. Liu et al., *Journal of the American Chemical Society* **138**, 5441 (2016), PMID: 27054904.
- [19] Y.-C. Chen et al., *Journal of the American Chemical Society* **138**, 2829 (2016), PMID: 26883386.
- [20] F.-S. Guo et al., *Science* **362**, 1400 (2018).
- [21] K. R. Meihaus and J. R. Long, *Dalton Trans.* **44**, 2517 (2015).
- [22] J. D. Rinehart and J. R. Long, *Journal of the American Chemical Society* **131**, 12558 (2009), PMID: 19689136.
- [23] N. Magnani et al., *Angewandte Chemie International Edition* **50**, 1696 (2011).
- [24] C. A. Gaggioli and L. Gagliardi, *Inorganic Chemistry* **57**, 8098 (2018), PMID: 29968473.
- [25] F. Neese and D. A. Pantazis, *Faraday Discuss.* **148**, 229 (2011).
- [26] G. A. Craig and M. Murrie, *Chem. Soc. Rev.* **44**, 2135 (2015).
- [27] L. Ungur and L. F. Chibotaru, *Inorganic Chemistry* **55**, 10043 (2016), PMID: 27508399.
- [28] F.-S. Guo, A. K. Bar, and R. A. Layfield, *Chemical Reviews* **119**, 8479 (2019), PMID: 31059235.
- [29] D. Hait, N. M. Tubman, D. S. Levine, K. B. Whaley, and M. Head-Gordon, *Journal of Chemical Theory and Computation* **15**, 5370 (2019), PMID: 31465217.
- [30] J. Shee, M. Loipersberger, D. Hait, J. Lee, and M. Head-Gordon, *The Journal of Chemical Physics* **154**, 194109 (2021).
- [31] B. O. Roos, P. R. Taylor, and P. E. Sigbahn, *Chemical Physics* **48**, 157 (1980).
- [32] P. E. M. Siegbahn, J. Almlöf, A. Heiberg, and B. O. Roos, *The Journal of Chemical Physics* **74**, 2384 (1981).
- [33] C. Angeli, R. Cimiraglia, S. Evangelisti, T. Leininger, and J.-P. Malrieu, *The Journal of Chemical Physics* **114**, 10252 (2001).
- [34] C. Angeli, R. Cimiraglia, and J.-P. Malrieu, *The Journal of Chemical Physics* **117**, 9138 (2002).
- [35] K. Andersson, P. A. Malmqvist, B. O. Roos, A. J. Sadlej, and K. Wolinski, *The Journal of Physical Chemistry* **94**, 5483 (1990).
- [36] K. Andersson, P. Malmqvist, and B. O. Roos, *The Journal of Chemical Physics* **96**, 1218 (1992).
- [37] J. Finley, P. Åke Malmqvist, B. O. Roos, and L. Serrano-Andrés, *Chemical Physics Letters* **288**, 299 (1998).
- [38] D. Ganyushin and F. Neese, *The Journal of Chemical Physics* **125**, 024103 (2006).
- [39] P. Åke Malmqvist, B. O. Roos, and B. Schimmelpfennig, *Chemical Physics Letters* **357**, 230 (2002).

- [40] S. Zhang and H. Krakauer, *Phys. Rev. Lett.* **90**, 136401 (2003).
- [41] W. A. Al-Saidi, S. Zhang, and H. Krakauer, *J. Chem. Phys.* **124**, 224101 (2006).
- [42] B. Eskridge, H. Krakauer, H. Shi, and S. Zhang, *The Journal of Chemical Physics* **156**, 014107 (2022).
- [43] K. T. Williams et al., *Phys. Rev. X* **10**, 011041 (2020).
- [44] J. Shee et al., *Journal of Chemical Theory and Computation* **15**, 2346 (2019), PMID: 30883110.
- [45] B. Rudsteyn et al., *Journal of Chemical Theory and Computation* **16**, 3041 (2020), PMID: 32293882.
- [46] B. Rudsteyn et al., *Journal of Chemical Theory and Computation* **18**, 2845 (2022), PMID: 35377642.
- [47] B. Eskridge, H. Krakauer, and S. Zhang, *Journal of Chemical Theory and Computation* **15**, 3949 (2019), PMID: 31244125.
- [48] P. C. Bunting et al., *Science* **362**, eaat7319 (2018).
- [49] M. Motta and S. Zhang, *WIREs Computational Molecular Science* **8**, e1364 (2018).
- [50] H. Shi and S. Zhang, *The Journal of Chemical Physics* **154**, 024107 (2021).
- [51] D. Thouless, *Nuclear Physics* **21**, 225 (1960).
- [52] W. Purwanto, H. Krakauer, Y. Virgus, and S. Zhang, *J. Chem. Phys.* **135**, 164105 (2011).
- [53] H. F. Trotter, *Proc. Am. Math. Soc.* **10**, 545 (1959).
- [54] M. Suzuki, *Commun. Math. Phys.* **51**, 183 (1976).
- [55] R. D. Stratonovich, *Dokl. Akad. Nauk. SSSR* **115**, 1907 (1957).
- [56] J. Hubbard, *Phys. Rev. Lett.* **3**, 77 (1959).
- [57] S. Zhang, *Auxiliary-field quantum monte carlo at zero- and finite-temperatures*, edited by E. Pavarini, E. Koch, and S. Zhang (Verlag des Forschungszentrum Jülich, 2019), Vol. **9**.
- [58] W. Purwanto, S. Zhang, and H. Krakauer, *J. Chem. Phys.* **130**, 094107 (2009).
- [59] F. Ma, S. Zhang, and H. Krakauer, *New Journal of Physics* **15**, 093017 (2013).
- [60] T. J. Pearson, M. S. Fataftah, and D. E. Freedman, *Chem. Commun.* **52**, 11394 (2016).
- [61] S. C. Coste, B. Vlasisavljevich, and D. E. Freedman, *Inorganic Chemistry* **56**, 8195 (2017), PMID: 28661134.
- [62] W. Purwanto, S. Zhang, and H. Krakauer, *Journal of Chemical Theory and Computation* **9**, 4825 (2013), PMID: 26583401.
- [63] B. A. Heß, C. M. Marian, U. Wahlgren, and O. Gropen, *Chemical Physics Letters* **251**, 365 (1996).
- [64] T. E. H. Walker and W. G. Richards, *The Journal of Chemical Physics* **52**, 1311 (1970).
- [65] J. Netz, A. O. Mitrushchenkov, and A. Köhn, *Journal of Chemical Theory and Computation* **17**, 5530 (2021), PMID: 34388346.

- [66] A. A. Holmes, N. M. Tubman, and C. J. Umrigar, *Journal of Chemical Theory and Computation* **12**, 3674 (2016), PMID: 27428771.
- [67] S. Sharma, A. A. Holmes, G. Jeanmairet, A. Alavi, and C. J. Umrigar, *Journal of Chemical Theory and Computation* **13**, 1595 (2017), PMID: 28263594.
- [68] B. Mussard and S. Sharma, *Journal of Chemical Theory and Computation* **14**, 154 (2018), PMID: 29202220.
- [69] I. G. Rau et al., *Science* **344**, 988 (2014).
- [70] M. M. Hurley, L. F. Pacios, P. A. Christiansen, R. B. Ross, and W. C. Ermler, *The Journal of Chemical Physics* **84**, 6840 (1986).
- [71] S. F. Boys, *Rev. Mod. Phys.* **32**, 296 (1960).
- [72] J. Shee, S. Zhang, D. R. Reichman, and R. A. Friesner, *Journal of Chemical Theory and Computation* **13**, 2667 (2017), PMID: 28481546.
- [73] W. Purwanto and S. Zhang, *Phys. Rev. E* **70**, 056702 (2004).
- [74] M. Motta and S. Zhang, *Journal of Chemical Theory and Computation* **13**, 5367 (2017), PMID: 29053270.
- [75] S. Chen and S. Zhang, Computation of forces and stresses in solids: towards accurate structural optimizations with auxiliary-field quantum monte carlo, <https://arxiv.org/abs/2302.07460>, 2023.
- [76] J. Shee, E. J. Arthur, S. Zhang, D. R. Reichman, and R. A. Friesner, *Journal of Chemical Theory and Computation* **14**, 4109 (2018), PMID: 29897748.
- [77] F. D. Malone, S. Zhang, and M. A. Morales, *Journal of Chemical Theory and Computation* **16**, 4286 (2020), PMID: 32437147.
- [78] A. Mahajan, J. Lee, and S. Sharma, *The Journal of Chemical Physics* **156**, 174111 (2022).